Chemical Science

ROYAL SOCIETY OF CHEMISTRY

EDGE ARTICLE

View Article Online
View Journal | View Issue

Cite this: *Chem. Sci.*, 2022, **13**, 12426

All publication charges for this article have been paid for by the Royal Society of Chemistry

Femtosecond anisotropy excitation spectroscopy to disentangle the Q_x and Q_y absorption in chlorophyll *a*†

Clark Zahn,* Till Stensitzki‡ and Karsten Heyne *

Chlorophyll *a* (Chl *a*) belongs to the most important and most investigated molecules in the field of photosynthesis. The Q-band absorption is central for energy transfer in photosystems and the relative orientation of the Q_y transitions of interacting chlorophylls governs the energy transfer. Chl *a* was well investigated, but a quantitative separation of Q_x and Q_y contributions to the Q-band of the Chl *a* absorption spectrum is still missing. We use femtosecond Vis-pump – IR-probe anisotropy excitation spectroscopy to disentangle the overlapping electronic Q_x and Q_y contributions quantitatively. In an anisotropy excitation spectrum we trace the dichroic ratio of a single vibration, *i.e.* the keto C=O stretching vibration at 1690 cm^{-1}, as a function of excitation wavelength. The change in dichroic ratio reflects altering Q_y and Q_x contributions. We identified Q_{x00} (0–0 transition of Q_x) and Q_{x01} transition at (636 ± 1) nm and (607 ± 2) nm, respectively, and the Q_{y01} and Q_{y02} at (650 ± 6) nm, and (619 ± 3) nm, respectively. We find that Q_x absorption, contributes to 50% to 72% at 636 nm and 49% to 71% at 606 nm to the Chl *a* absorption at room temperature. The Q band was well modelled by a single vibronic progression for the Q_x and Q_y transition of (700 ± 100) cm^{-1}, and the energy gap between Q_{x00} and Q_{y00} was found to be (820 ± 60) cm^{-1}. This precise description of the hexa-coordinated Chl *a* absorption spectrum will foster more accurate calculations on energy transfer processes in photosystems, and advance the detailed understanding of the intricate interaction of chlorophyll molecules with the solvent.

Received 24th June 2022
Accepted 30th September 2022

DOI: 10.1039/d2sc03538c

rsc.li/chemical-science

1 Introduction

Absorption spectra of many important molecules such as photoreceptors, metal complexes and different kinds of tetrapyrroles, including chlorophylls, show spectrally overlapping contributions of different electronic transitions. A clear identification of the contributions at a given wavelength is typically connected with calculations in combination with measurements at different experimental conditions.[1–4] However, the interpretation of the experimental results depends strongly on the calculations, which become increasingly difficult for larger molecules. Here, we demonstrate a method based on polarization resolved femtosecond Vis-pump IR-probe spectroscopy to disentangle spectral contributions of different electronic transitions in the electronic ground state, without requiring theoretical calculations. As an application example we have chosen the decomposition of the Q-band of chlorophyll *a* (Chl *a*).

Chl *a* plays a fundamental role in photosynthesis, from the initial energy transfer in the light harvesting complex to the electron transfer in the reaction center.[5] In order to understand the different photosynthetic processes, an understanding of Chl *a* and its photophysical properties is crucial. Chl *a* shares many properties with other cyclic tetrapyrroles. As described by the Gouterman Model,[6] its chlorin macrocycle gives rise to two distinct broad absorption bands: the soret (B)-band at 350 nm to 450 nm and the Q-band at 550 nm to 680 nm. In addition, both the B- and the Q-band are further comprised of two distinguishable electronic states with different geometrical orientations: B_x, B_y and Q_x, Q_y.[7] Here, *x* and *y* indicate the expected directions of the transition dipole moments (tdm) for the transition between the ground-state and the respective excited-state within the chlorophylls macrocycle plane as depicted in Fig. 1 inset.

Particularly, the Q-band plays a key role in the efficient energy transport.[5] Thus, its physical properties are widely studied using different experimental techniques, including linear dichroism,[8–10] circular dichroism and magnetic circular dichroism (MCD),[1,11–17] spectral hole-burning[18,19] and

Department of Physics, Free University Berlin, Arnimallee 14, D-14195 Berlin, Germany. E-mail: lark.zahn@fu-berlin.de; karsten.heyne@physik.fu-berlin.de; clark.zahn@fu-berlin.de; Tel: +49 30 838 56107

† Electronic supplementary information (ESI) available. See DOI: https://doi.org/10.1039/d2sc03538c

‡ Present address: Institute of Chemistry, University of Potsdam, Karl-Liebknecht-Str. 24-25, 14476 Potsdam-Golm, Germany.

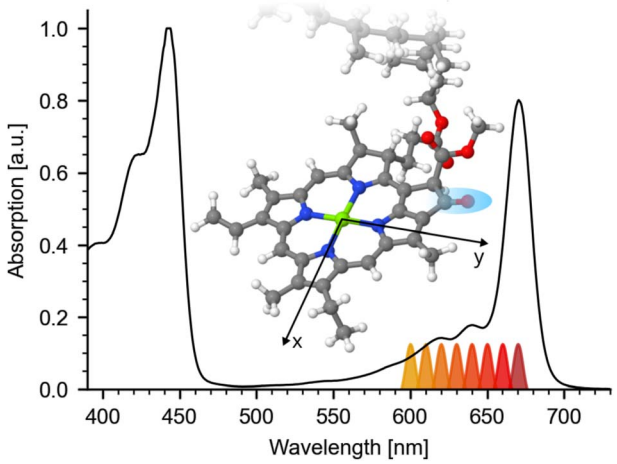

Fig. 1 Visible steady state absorption of hexa-coordinated Chl *a* in pyridine. The spectrum is normalized to its Soret-band at 443 nm. Q-band absorption is exhibiting a maximum at 670 nm followed by a shoulder around 644 nm and high energy side peaks at 619 nm and 585 nm. Different excitation wavelengths for the pump-pulse are indicated below the spectrum. Inset: Geometry optimized structure of Chl *a* macrocycle with *x* and *y* axis (taken from ref. 25). Atoms are color coded: carbon (gray), nitrogen (blue), magnesium (green), oxygen (red), and hydrogen (white). The investigated keto C=O group is marked by a blue region.

fluorescence spectroscopy,[20–22] as well as different time-resolved transient absorption[23–25] and 2D-absorption measurements.[2,26,27] Despite extensive research, the exact composition of the Q-band absorption is not yet fully understood. Even though, the low energetic Q_y 0–0 transition (Q_{y00}) could be assigned to the prominent low energy peak of the Q-band at 660 nm to 670 nm early on,[8,10–13] particularly the assignment of the Q_x transition long remained controversial,[1,8,10–17,19,20] with different assignment options being considered. Moreover, changes in the macrocycle conformation, induced by penta- or hexa-coordination, induce a shift of the Q_x band position of Chl *a*,[14,17,20] complicating conclusive assignment. Yet, only in the last decade, new qualitative information on the spectral position of Q_x and Q_y was obtained.[17,20] Furthermore, different polarisation resolved studies using femtosecond Vis-pump VIS-probe and 2DES spectroscopy investigated the spectral contributions of Q_x and Q_y.[2,23,24] They show strong polarization dependence as a function of probing and pumping wavelengths. Unfortunately, the broad excited state absorption (ESA) of Chl *a* with different anisotropic contributions,[23] together with the broad bleaching (BL) and stimulated emission contributions makes the interpretation very difficult without simplifications.[2] Yet, despite different approaches, up to now, to our knowledge no quantitative disentangling of Q_x and Q_y contributions was reported, so that the exact Q_x and Q_y absorption spectrum remains unknown.

Here, we apply anisotropy excitation spectroscopy tracing the impact of electronic excitation on the vibrational anisotropy at different excitation wavelengths. Compared to probing electronic transitions, the much narrower line-width and the multitude of vibrational bands enable a precise measurement of anisotropy changes. However, even though in nature Chl *a* are largely penta-coordinated,[28,29] the two diastereotopic faces (*syn* and *anti*) of penta-coordinated Chl *a*,[30,31] make an unambiguous analysis of anisotropy changes difficult. Thus, using hexa-coordinated Chl *a* in pyridine allows for a clear analysis of its anisotropy excitation spectrum, providing a first clear separation of the Q_x and Q_y absorption spectra and a giving a more in-depth understanding of the electronic structure of Chl *a*.

2 Materials and methods

2.1 Sample preparation

Chl *a* from spinach was purchased from Sigma-Aldrich. All samples were dissolved in pyridine and prepared in sample cells with a thickness of 100 μm, with a sample concentration of 1.5 mM to 3 mM (corresponding to an absorption of ~2.5 OD at 671 nm). In pyridine, Chl *a* is hexa-coordinated and has a flat macrocycle.[14,20,32,33]

2.2 Transient absorption

Femtosecond laser pulses were generated starting from pulses delivered by a 1.088 kHz Ti:Sa laser system (Coherent Legend USP, 80 fs pulses at 808 nm). Spectrally tunable visible pump pulses were generated by cascaded OPAs generating fs output pulses of ~6 μJ and (130 ± 20) fs. In detail, a collinear BBO OPA pumped at 400 nm generated near-IR pulses at 1200 nm to 1350 nm, which were further amplified by two KTA amplification stages pumped with the fundamental at 800 nm. The near-IR pulses were then frequency doubled in a BBO-crystal, generating desired pump wavelengths between 600 and 670 nm with a spectral width of FWHM (10 ± 3) nm. A filter (Schott KG4) and a polarizer removed the remaining near-IR frequencies. To ensure photoselection conditions, the pump-pulses were further attenuated to 0.2 μJ to 0.5 μJ, exciting less than 20% of the sample. A λ/2-plate was used to set the polarization of the pump-beam, alternating between perpendicular and parallel pump – probe configuration. The diameter of the pump beam on the sample was (220 ± 40) μm (FWHM), the diameter of the two probe beams on the sample was (150 ± 30) μm (FWHM).

IR probe beams with energies 50 nJ were generated as reported elsewhere.[34] Two reflections of the fs mid-IR pulse were taken, one as probe beam and one as reference. Both beams pass through the same sample volume, with the reference pulse arriving 1.5 ns before the probe, further reducing the shot-to-shot noise.[35] The system response duration was about (300 ± 50) fs. Both IR pulses are detected by dispersing the beams with an imaging spectrograph and recording both beams simultaneously with a 2 × 32 element MCT-array from Infrared Associates. The spectral resolution was better than 3 cm^{-1}. The sample was moved with a Lissajous-scanner to ensure a fresh sample volume between consecutive pump pulses. The probe pulses were delayed using a mechanical translation stage.

We excited the isotropic Chl *a* solution with linear polarized excitation pulses introducing a sub-set of oriented excited Chl *a* molecules (photoselection). This generates a transient anisotropy in the sub-set of excited molecules, which decays

through rotational diffusion with $\tau \sim 90$ ps.[25] On a time-scale between 5 to 15 ps the change in anisotropy of the keto C=O stretching vibration is negligible within the S/N (see ESI Fig. SI 1†).

In Vis-pump IR-probe experiments, only signals from the excited sub-sets are detected. With polarization resolved mid-IR probing, the dichroic ratio D is given by $D = \frac{A_{\parallel}}{A_{\perp}}$ for signal amplitudes of parallel $A_{\parallel}$ and perpendicular $A_{\perp}$ polarizations with respect to pump-pulse polarization. The ratio of the probed amplitudes reflect the projection of the vibrational tdm onto the excited electronic tdm. In particular, the relative angle θ between the excited and probed tdm is given by $\theta = \arccos(\sqrt{(2D-1)/(D+2)})$.

3 Results and discussion

Steady state absorption of Chl *a* in pyridine is shown in Fig. 1, displaying Soret-band absorption at 390 nm to 460 nm and Q-band absorption at 570 nm to 670 nm. We performed photo-selection experiments creating an oriented sub-set of excited Chl *a* molecules and probed their dynamics by polarization resolved mid-IR spectroscopy. Photoexcitation of the Q-band initiates ultrafast 100 fs to 200 fs dynamics assigned to internal conversion from Q_x to Q_y,[2,23,24,26] followed by population of the Q_y state, decaying on a nanosecond time-scale,[5] with negligible amplitude changes from 0.4 ps to 15 ps (see ESI Fig. SI 1†). Absorption spectra for different excitation wavelengths averaged over delay times from 5 ps to 15 ps are displayed in Fig. 2. Parallel and perpendicular polarizations with respect to the pump-polarization are shown in black and red, respectively. The spectral region of the keto C=O stretching vibration shows a prominent bleaching (BL) signal at 1690 cm^{-1} and an associated excited state absorption (ESA) at 1650 cm^{-1}.[36] Upon visible excitation at the low energy side of the Q-band at 670 nm, a pure Q_y contribution is observed.[8,10–13] In this case, the observed dichroic ratio D (670 nm) is around 2.59, with a 1σ range from 2.47 to 2.73. This value corresponds to a relative angle θ of $(18 \pm 3)^\circ$ between the keto C=O vibrational tdm and the Q_y tdm in agreement with earlier findings.[37]

Upon excitation at shorter wavelengths the dichroic ratio decreases from 2.4 at 660 nm to 1.6 at 640 nm. Going to even shorter wavelengths, the ratio increases until 620 nm, then decreases again at wavelength of 600 nm. Since, the dichroic ratio is fixed for a given electronic transition,[38] this twofold decrease indicates two distinct contributions of another electronic transition, *i.e.* the Q_x transition. The dichroic ratio changes by about 1 as a function of excitation wavelengths, presenting a high anisotropy contrast for the keto C=O stretching vibration in connection to Q-band transitions. Thus, the keto C=O stretching vibration provides a well suited marker band for anisotropy excitation spectroscopy of Chl *a*.

We modelled the keto C=O ESA and BL signals for both polarizations simultaneously with a sum of Lorentzians, as depicted in Fig. 2. Since the dichroic ratio of the vibrational transition is expected to be identical for the BL and ESA band in a rigid molecule,[39] we further constrained the fit by modeling both BL and ESA band with the same dichroic ratio. Errors are calculated using exhaustive search analysis.[39,40] The resulting changes in the dichroic ratio or anisotropy of the keto C=O vibration as a function of excitation wavelength are displayed in the excitation spectrum in Fig. 3a.

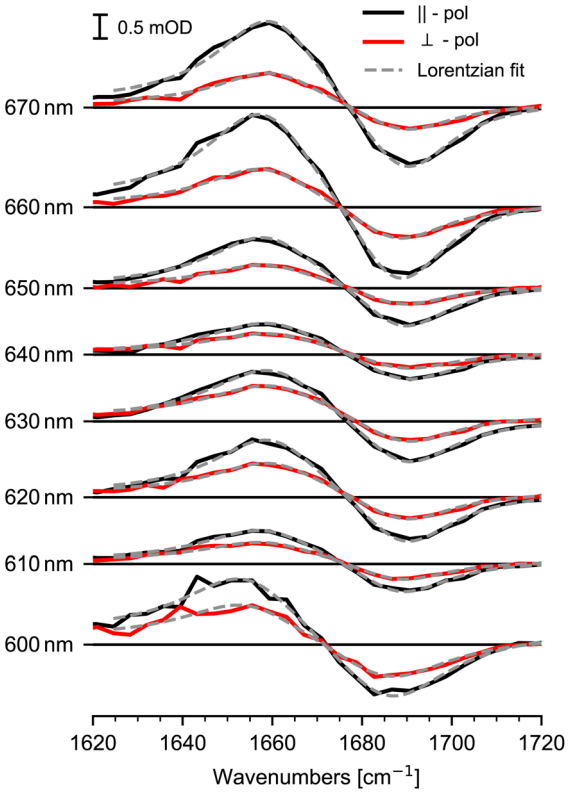

Fig. 2 Transient mid-IR absorption spectra of the keto C=O stretching vibration for different excitation wavelengths averaged over delay times from 5 ps to 15 ps for parallel (black) and perpendicular (red) polarization orientation. Bleaching (negative) signals at 1690 cm^{-1} reflect the keto C=O stretching vibration in the electronic ground state and (positive) signals at 1650 cm^{-1} display excited state signals in the Q_y state. The orientation of the detected sub-set is induced by the effective tdm given by the mixture of excited Q_x and Q_y tdms. Lorentzian fits are presented by gray dashed lines.

3.1 Q_x contribution in the Chl *a* spectrum

Changes in anisotropy directly mirror altering contributions of excited electronic transitions. The dichroic ratio D and anisotropy r can be used interchangeably ($r = (D-1)/(D+2)$). Here, the dichroic ratio is directly obtained from modelling the data (see Fig. 3a). Thus, in order to unravel the Q_x and Q_y absorption, it is convenient to work with the dichroic ratio. For two contributing transitions Q_x and Q_y, the dichroic ratio for different excitation wavelengths $D(\lambda)$ is a linear combination of the corresponding Q_x and Q_y dichroic ratios D_{Q_x} and D_{Q_y}:

$$D(\lambda) = (1 - c(\lambda))D_{Q_y} + c(\lambda)D_{Q_x} \quad (1)$$

with $c(\lambda)$ being the relative contribution of the Q_x transition between zero and one, and $1 - c(\lambda)$ being the relative

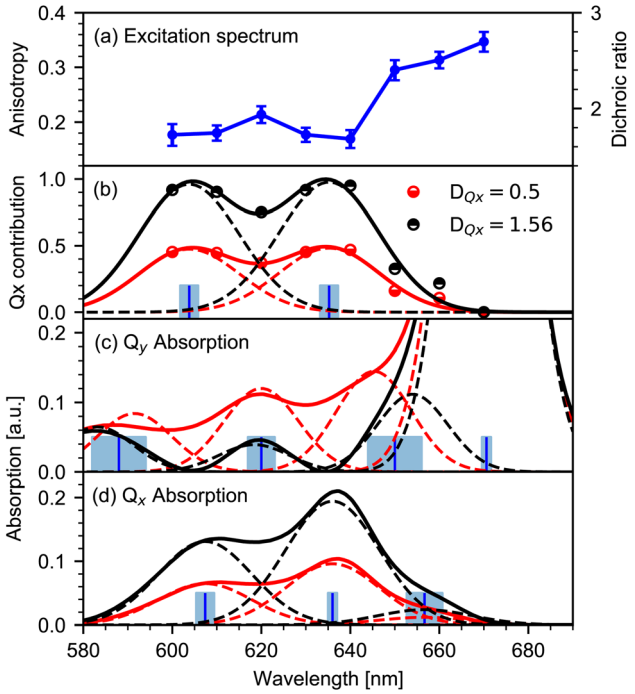

Fig. 3 Mapping the Q_x and Q_y absorption spectrum from the anisotropy excitation spectrum. (a) Excitation spectrum of the keto C=O stretching vibration (blue dots) as a function of excitation wavelength. Left scale anisotropy, right scale dichroic ratio. Errors (1σ ranges) are presented for the dichroic ratio. (b) Contribution $c(\lambda)$ of the Q_x-transition to the Chl *a* absorption spectrum at different wavelengths (dots) calculated from (a). Modelling of $c(\lambda)$ (solid lines) by two Gaussian peaks (dashed lines) for two limiting D_{Q_x} values of 1.56 (black) and 0.5 (red). Blue bars represent the center of the Gaussians. Error ranges for D_{Q_x} values of 1.56 and 0.5 are indicated in light blue. (c) Q_y absorption spectrum (product of Chl *a* absorption spectrum with $(1 - c(\lambda))$, solid lines) for the two limiting D_{Q_x} values (same color code as in b). Modelled spectrum by four Gaussians (dashed lines) with identical widths, and peaks Q_{y00} at (671 ± 1) nm, Q_{y01} at (650 ± 6) nm and Q_{y02} at (619 ± 3) nm. Note, that the last peak at (588 ± 6) nm is not covered by the anisotropy excitation experiment. (d) Q_x absorption spectrum (product of $c(\lambda)$ with the Chl *a* absorption spectrum, solid lines) for the two limiting D_{Q_x} values (same color code as in b). Modelled spectrum with three Gaussians (dashed lines) with identical widths and peaks Q_{x00} at (636 ± 1) nm, Q_{x01} at (607 ± 2) nm, and Q_{x10} at (657 ± 4) nm.

contribution of the Q_y transition. The relative contribution $c(\lambda)$ of the Q_x transition to the absorption spectrum is given by:

$$c(\lambda) = \frac{D(\lambda) - D_{Q_y}}{D_{Q_x} - D_{Q_y}} \quad (2)$$

In general, the dichroic ratio of a band can vary between 0.5 and 3. However, since the Q_x contribution cannot exceed 100%, the largest possible value of D_{Q_x} is 1.56 (see Fig. 3a), therefore limiting the range of D_{Q_x} to 0.5 to −1.56.

For the limiting values of D_{Q_x}, the relative Q_x contribution $c(\lambda)$ is presented in Fig. 3b (dots). In the observed range, the relative contribution $c(\lambda)$ exhibits two peaks at around 635 nm and 605 nm. We modelled the relative contribution $c(\lambda)$ of Q_x with two Gaussians centered at (635 ± 2) nm and (604 ± 2) nm, as depicted in Fig. 3b (solid lines). Contributions below 600 nm are needed to model the data. Note that for wavelengths below 600 nm the significance of the modelled contribution *c* decreases rapidly to shorter wavelengths.

3.2 Extracting pure Q_x and Q_y absorption spectra

The individual Q_y and Q_x absorption spectra are calculated by the product of the Chl *a* absorption spectrum (normalized to the Q-band maximum at 670 nm) with the modelled contributions of Q_y $(1 - c(\lambda))$ and Q_x as shown in Fig. 3b. The resulting absorption spectra of the pure Q_y and Q_x transitions for the limiting D_{Q_x} values of 0.5 and 1.56 are depicted in Fig. 3c and d, respectively.

3.3 Analysis of the Q_y absorption spectrum

Modelling the Q_y absorption spectrum with Gaussians of the same spectral widths yields peaks at (670 ± 2) nm, (648 ± 5) nm and (617 ± 2) nm (dashed lines in Fig. 3c). We assign the peak at 671 nm to the 0–0 transition Q_{y00} and the remaining two peaks to one vibronic progression with 0–1 transition Q_{y01} at 650 nm and 0–2 transition Q_{y02} at 619 nm. The frequency differences between adjacent Q_y peaks is (700 ± 200) cm^{-1}.

In order to model the data, an additional peak at shorter wavelength is needed, yielding a peak position at and (588 ± 6) nm. As the peak is out of the spectral range of our measured anisotropy excitation spectrum, it is not possible to determine its exact contribution to the absorption spectrum. However, the spectral position matches the vibronic progression of (700 ± 200) cm^{-1}, suggesting possible 0–3 transition Q_{y03} at (588 ± 6) nm.

Spectroscopic investigations[24,26] on penta-coordinated Chl *a* revealed coherent oscillations with a frequency of about 700 cm^{-1}, showing a substantial coupling between vibrational modes and electronic excitations in this spectral range. Moreover, hole-burning fluorescence spectroscopy revealed vibrational contributions around 700 cm^{-1} for penta- and hexa-coordinated Chl *a*.[20] The peak around (648 ± 5) nm was observed before, but was associated either to the Q_x transition[20] or to the Q_y transition.[10] With our method we can assign this peak to the Q_y transition.

3.4 Analysis of the Q_x absorption spectrum

The Q_x absorption spectrum is shown in Fig. 3d, displaying peaks at (657 ± 4) nm, (636 ± 1) nm and (607 ± 2) nm (dashed lines). We assign the peaks (636 ± 1) nm and (607 ± 2) nm to 0–0 transition Q_{x00}, and 0–1 transition Q_{x01} of the Q_x absorption, respectively. The very small peak around 657 nm is tentatively assigned to the 1–0 transition Q_{x10}. This contribution should be strongly temperature dependent. Spectral position and assignment of both Q_x and Q_y bands is summarized in Table 1.

The frequency difference between Q_{x00} and Q_{x01} is (700 ± 100) cm^{-1}, and between Q_{x10} and Q_{x00} is (500 ± 200) cm^{-1}. Thus, a vibronic progression in the Q_x absorption spectrum with a frequency around 700 cm^{-1} seems plausible.

Table 1 Spectral position of Q_x and Q_y absorption bands

Peak [nm]	Peak [cm^{-1}]	Assignment
671 ± 1	14 900 ± 30	Q_{y00}
657 ± 4	15 220 ± 100	Q_{x10}[a]
650 ± 6	15 400 ± 150	Q_{y01}
636 ± 1	15 720 ± 30	Q_{x00}
619 ± 3	16 160 ± 80	Q_{y02}
607 ± 2	16 480 ± 60	Q_{x01}

[a] Thermally excited ground state.

3.5 Vibronic progressions

The vibronic progression frequency of Q_x match the one from the Q_y transitions. Thus, we propose a single vibronic progression of about 700 cm^{-1} in the Q_x and Q_y absorption spectra. Other more complex interpretations are possible, but our simple model explains the spectroscopic findings in the absorption spectrum reasonably. From our analysis, the $Q_y - Q_x$ energy gap is (820 ± 60) cm^{-1}, matching the reported value of about 875 cm^{-1},[20] and compatible with 970 cm^{-1}.[1] The energy gap is close to the frequency of the vibronic progression, making it difficult to reliably determine the contributions from the visible spectra alone. In this context we interpret the reported value of 1294 cm^{-1} for the vibronic progression.[10]

3.6 Refined absorption spectra

Up to this point, no additional information on the relative orientations of the electronic tdms were taken into account. Following the generally accepted Gouterman Model,[6] the relative angle between the Q_x and Q_y tdm is expected to be close to 90°. This is confirmed by experimental studies on hexa- and penta-coordinated Chl *a* reporting angles between Q_y and Q_x tdm of about 70° to 74°.[2,10] If we assume the angle between Q_y and Q_x tdm to be in the range of 70° to 90°, and combine this information with a maximal angle of 20° between the keto C=O tdm and Q_y tdm ($D_{+1\sigma}$(670 nm) = 2.47 ≙ 20°), we get a maximal relative angle range of 50° to 90° between keto C=O tdm and Q_x tdm. This correspond to a value range of D_{Q_x} = 0.5–1.15. Taking this into account, the disentangled Q_x and Q_y absorption spectra of Chl *a* in pyridine and their possible variation due to different D_{Q_x} values are presented in Fig. 4. The sum of Q_x and Q_y spectra of corresponding D_{Q_x} values give the measured Chl *a* absorption spectrum. We find that the Q_x contribution to the Chl *a* Q-band absorption spectrum between 590 nm and 700 nm is always smaller than (72 ± 5)%, and is in the range of 50% to 72% at 636 nm and of 49% to 71% at 606 nm.

Using the disentangled absorption spectrum, we can determine the oscillator strength ratio between $f(Q_x)$ and $f(Q_y)$. With normalized Q_{y00} absorption at 671 nm and Q_{x00} absorption strength at f(636 nm) = 0.14 ± 0.04, the ratio $f(Q_x)/f(Q_y)$ is between 5.6–10. This is in agreement with a value of 5.9 reported for Chl *a* in pyridine[1] and with a value of 7.5 for penta-coordinated Chl *a* in ethanol.[24] In addition, from the relative intensities of the Q_x and Q_y absorption bands, we calculated the relative Franck–Condon factors (see Table 2) in agreement with earlier findings.[10]

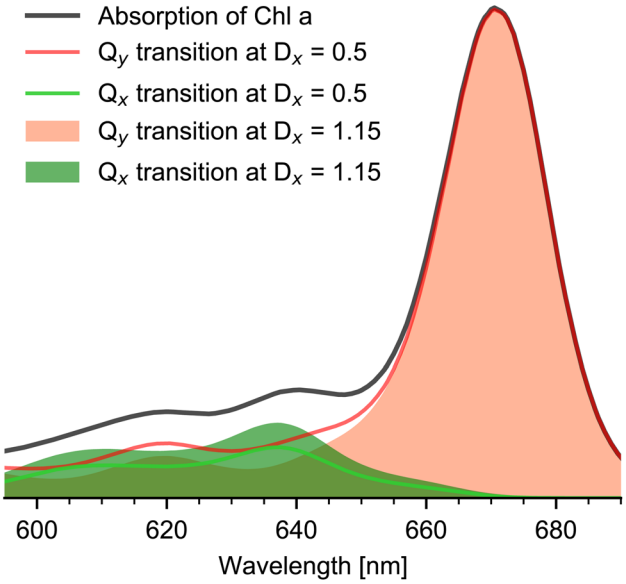

Fig. 4 Chl *a* absorption spectrum and Q_x and Q_y contributions. Hexa-coordinated Chl *a* absorption spectrum (black line) in pyridine solution and Q_y (orange) and Q_x (green) absorption spectra for the two limiting D_{Q_x} values 0.5 (minimal, solid lines) and 1.15 (maximal, filled area). The sum of Q_x and Q_x spectra at the same D_{Q_x} value gives the experimental Chl *a* absorption spectrum.

3.7 Discussion

The optical properties of Chl *a* are strongly affected by temperature, macrocycle coordination, and interaction with solvent molecules.[14,20,32,41,42] In the gas phase recent calculations report a $Q_x - Q_y$ energy gap of 2400 cm^{-1}.[43] In condensed phase the energy gap was reported to be around 900 cm^{-1},[1,20] matching our findings of (820 ± 60) cm^{-1}. The fraction of Q_x contribution to the Chl *a* absorption spectrum was estimated between 10% to 25% (ref. 1) in agreement with our findings of 14% to 27% in the spectral region from 590 nm to 720 nm.

Moreover, a strong vibronic coupling was predicted that inseparably mixes Q_x and Q_y transitions.[1] From our measurements we can state that such a mixing has no or negligible effect on the orientation of the electronic tdms, since the tdms are well distinguishable and are the cause for our observed anisotropy contrast. Hence, the orientation of the excited electronic Q_x tdm is preserved on a hundred picosecond time-scale. Upon Q_x excitation, ultrafast energy relaxation to Q_y is reported, with a time constant of 150 fs to 200 fs.[2,23,24,26] We found that excitation of Chl *a* in the spectral range between 606 nm and 636 nm leads to an approximate 1 : 1 excitation of Q_x and Q_y transitions. Thus, excitation with linear polarized light generates populated

Table 2 Relative Franck–Condon factors of the Q_x and Q_y transition calculated from the calculated Q_y and Q_x absorption spectra, see Fig. 3c and d (dashed lines), respectively)

Q_x	Q_y
$(Q_{x00} : Q_{x01})$ nm = 1.5 ± 0.2	$(Q_{y00} : Q_{y01})$ nm = 7 ± 2
—	$(Q_{y00} : Q_{y02})$ nm = 9 ± 3

Q_y states along the *x*- and *y*-axis direction. This is essential for simulating energy transfer processes at various excitation wavelengths in photosystems, *e.g.* in LHC II.[37,44,45]

We localized the Q_{x00} transition at 636 nm. For wavelength longer than 650 nm only the Q_y transition contributes to the Chl *a* spectrum, revealing a shoulder at (650 ± 6) nm. Up to now, this shoulder remained largely unnoticed, leading prior studies to locate the Q_{y01} at 613 nm to 619 nm.[1,10,20] We assign the Q_{y01} to the peak at (650 ± 6) nm.

Consequently, in contrast to earlier findings, we explain the substructure of the absorption spectrum of the hexa-coordinated Chl *a* between 600 nm to 720 nm by a single vibronic progression with a frequency of about 700 cm^{-1}.

4 Conclusion

Femtosecond Vis-pump – IR-probe anisotropy excitation spectroscopy is an efficient tool to identify spectral positions and contributions of different electronic transitions within the electronic absorption spectrum. Tracing the pump wavelength dependence of vibrational anisotropy allows for separation of electronic transitions with distinct tdm orientations.

Applying this method on hexa-coordinated Chl *a*, we separated Q_x and Q_y contributions to the Q-band absorption quantitatively, with 0–0 transition of Q_y (Q_{y00}) at (671 ± 1) nm, and Q_{x00} at (636 ± 1) nm. The investigated spectral Q-band range is well modelled by a single vibronic progression with a single frequency of 700 cm^{-1} for both the Q_x and the Q_y transition. We clearly identified the Q_{y01} and Q_{y02} vibronic progression peaks at (650 ± 6) nm, and (619 ± 3) nm, respectively, and the Q_{x01} peak at (607 ± 2) nm. The Q_x and Q_y transition tdms are well separated and not mixed. The energy gap between Q_{x00} and Q_{y00} was specified to (820 ± 60) cm^{-1}. We identified distinct relative Franck–Condon factors for the Q_y and Q_x transitions. The ratio of Q_{y00} to Q_{y01}, and Q_{y02} is 7 ± 2 and 9 ± 3, respectively. In contrast the ratio of Q_{x00} to Q_{x01} is 1.5 ± 0.2, reflecting a substantially stronger vibronic coupling in the Q_x transition. The foundation for this contrast may be attributed to the difference in symmetry, but further studies need to explore the details of this contrast. We expect that extending the studies to multiple vibrational transitions may increase accuracy and provide more detailed information.

Our results provide an essential framework for further calculations of energy transfer processes on photosystems and a starting point for comparing Chl *a* properties with penta-coordinated macrocycle. Anisotropy excitation spectroscopy is a powerful and straight-forward tool to unravel different electronic ground-state transitions and their vibronic sub-structure in a variety of important photoactive molecules such as porphyrins, corroles, linear tetrapyrroles, metal complexes and photoreceptors.

Data availability

Data for this paper, including transient polarization resolved data are available at **https://box.fu-berlin.de/s/YbB4AamN4JZiYLB**.

Author contributions

K. H. designed the experiment; C. Z. performed the Vis-IR spectroscopy and analyzed the data, T. S. and K. H. contributed to analyzing the data, C. Z. and K. H. wrote the manuscript with input from all authors.

Conflicts of interest

There are no conflicts to declare.

Acknowledgements

We thank the Deutsche Forschungsgemeinschaft DFG 169703910 and SFB-1078 for financial support.

References

1 J. Reimers, Z.-L. Cai, R. Kobayashi, M. Rätsep, A. Freiberg and E. Krausz, *Sci. Rep.*, 2013, **3**, 2761.
2 Y. Song, A. Schubert, E. Maret, R. K. Burdick, B. D. Dunietz, E. Geva and J. P. Ogilvie, *Chem. Sci.*, 2019, **10**, 8143–8153.
3 F. Santoro, A. Lami, R. Improta, J. Bloino and V. Barone, *J. Chem. Phys.*, 2008, **128**, 224311.
4 M. S. Katelyn, J. Dasgupta, J. C. Lagarias and R. A. Mathies, *J. Am. Chem. Soc.*, 2009, **131**, 13946.
5 R. E. Blankenship, *Molecular mechanisms of photosynthesis*, Wiley-Blackwell, London, 2nd edn, 2014.
6 M. Gouterman, *J. Mol. Spectrosc.*, 1961, **6**, 138–163.
7 M. Gouterman and L. Stryer, *J. Chem. Phys.*, 1962, **37**, 2260–2266.
8 L. L. Shipman, T. M. Cotton, J. R. Norris and J. J. Katz, *J. Am. Chem. Soc.*, 1976, **98**, 8222–8230.
9 D. Bauman and D. Wrobel, *Biophys. Chem.*, 1980, **12**, 83–91.
10 M. Fragata, B. Norden and T. Kurucsev, *Photochem. Photobiol.*, 1988, **47**, 133–143.
11 C. Houssier and K. Sauer, *J. Am. Chem. Soc.*, 1970, **92**, 779–791.
12 C. Weiss, *J. Mol. Spectrosc.*, 1972, **44**, 37–80.
13 M. V. Belkov and A. P. Losev, *Spectrosc. Lett.*, 1978, **11**, 653–669.
14 M. Umetsu, Z.-Y. Wang, M. Kobayashi and T. Nozawa, *Biochim. Biophys. Acta, Bioenerg.*, 1999, **1410**, 19–31.
15 M. Umetsu, Z.-Y. Wang, K. Yoza, M. Kobayashi and T. Nozawa, *Biochim. Biophys. Acta, Bioenerg.*, 2000, **1457**, 106–117.
16 J. L. Hughes, R. Razeghifard, M. Logue, A. Oakley, T. Wydrzynski and E. Krausz, *J. Am. Chem. Soc.*, 2006, **128**, 3649–3658.
17 J. R. Reimers and E. Krausz, *Phys. Chem. Chem. Phys.*, 2014, **16**, 2315–2322.
18 R. Avarmaa and K. Rebane, *Spectrochim. Acta, Part A*, 1985, **41**, 1365–1380.
19 J. L. Hughes, B. Conlon, T. Wydrzynski and E. Krausz, *Phys. Procedia*, 2010, **3**, 1591–1599.
20 M. Rätsep, J. Linnanto and A. Freiberg, *J. Chem. Phys.*, 2009, **130**, 194501.

21 M. Rätsep, Z.-L. Cai, J. R. Reimers and A. Freiberg, *J. Chem. Phys.*, 2011, **134**, 024506.
22 M. Rätsep, J. M. Linnanto and A. Freiberg, *J. Phys. Chem. B*, 2019, **123**, 7149–7156.
23 P. Martinsson, J. A. Oksanen, M. Hilgendorff, P. H. Hynninen, V. Sundström and E. Åkesson, *Chem. Phys. Lett.*, 1999, **309**, 386–394.
24 Y. Shiu, Y. Shi, M. Hayashi, C. Su, K. Han and S. Lin, *Chem. Phys. Lett.*, 2003, **378**, 202–210.
25 M. Linke, A. Lauer, T. von Haimberger, A. Zacarias and K. Heyne, *J. Am. Chem. Soc.*, 2008, **130**, 14904–14905.
26 E. Meneghin, C. Leonardo, A. Volpato, L. Bolzonello and E. Collini, *Sci. Rep.*, 2017, **7**, 11389.
27 N. H. C. Lewis and G. R. Fleming, *J. Phys. Chem. Lett.*, 2016, **7**, 831–837.
28 P. Jordan, P. Fromme, H. Witt, O. Klukas, W. Saenger and N. Krauß, *Nature*, 2001, **411**, 909–917.
29 A. Ben-Shem, F. Frolow and N. Nelson, *Nature*, 2004, **426**, 630–635.
30 T. S. Balaban, P. Fromme, A. R. Holzwarth, N. Krauß and V. I. Prokhorenko, *Biochim. Biophys. Acta, Bioenerg.*, 2002, **1556**, 197–207.
31 M. O. Senge, A. A. Ryan, K. A. Letchford, S. A. MacGowan and T. Mielke, *Symmetry*, 2014, **6**, 781–843.
32 S. Krawczyk, *Biochim. Biophys. Acta, Bioenerg.*, 1989, **976**, 140–149.
33 K. Saito, T. Suzuki and H. Ishikita, *J. Photochem. Photobiol., A*, 2018, **358**, 422–431.
34 R. A. Kaindl, M. Wurm, K. Reimann, P. Hamm, A. M. Weiner and M. Woerner, *J. Opt. Soc. Am. A*, 2000, **17**, 2086–2094.
35 T. Stensitzki, Y. Yang, V. Kozich, A. A. Ahmed, F. Kössl, O. Kühn and K. Heyne, *Nat. Chem.*, 2018, **10**, 126–131.
36 A. S. Holt and E. E. Jacobs, *Plant Physiol.*, 1955, **30**, 553–559.
37 M. Kaucikas, K. Maghlaoui, J. Barber, T. Renger and J. Thor, *Nat. Commun.*, 2016, **7**, 13977.
38 Y. Yang, D. Jones, T. von Haimberger, M. Linke, L. Wagnert, A. Berg, H. Levanon, A. Zacarias, A. Mahammed, Z. Gross and K. Heyne, *J. Phys. Chem. A*, 2012, **116**, 1023–1029.
39 M. Theisen, M. Linke, M. Kerbs, H. Fidder, M. E.-A. Madjet, A. Zacarias and K. Heyne, *J. Chem. Phys.*, 2009, **131**, 124511.
40 M. Newville, T. Stensitzki, D. B. Allen and A. Ingargiola, *LMFIT: Non-Linear Least-Square Minimization and Curve-Fitting for Python*, 2014.
41 S. B. Broyde and S. S. Brody, *J. Chem. Phys.*, 1967, **46**, 3334–3340.
42 I. Renge and R. Avarmaa, *Photochem. Photobiol.*, 1985, **42**, 253–260.
43 A. Sirohiwal, R. Berraud-Pache, F. Neese, R. Izsák and D. A. Pantazis, *J. Phys. Chem. B*, 2020, **124**, 8761–8771.
44 L. O. Pålsson, M. D. Spangfort, V. Gulbinas and T. Gillbro, *FEBS Lett.*, 1994, **339**, 134–138.
45 Y. Shibata, S. Nishi, K. Kawakami, J.-R. Shen and T. Renger, *J. Am. Chem. Soc.*, 2013, **135**, 6903–6914.